Wearable Shell Antenna for 2.4 GHz Hearing Instruments

Ruaro, Andrea; Thaysen, Jesper; Jakobsen, Kaj Bjarne

Published in:
IEEE Transactions on Antennas and Propagation

Link to article, DOI:
10.1109/TAP.2016.2543800

Publication date:
2016

Document Version
Peer reviewed version

Wearable Shell Antenna for 2.4 GHz Hearing Instruments

Andrea Ruaro, Jesper Thaysen, and Kaj B. Jakobsen

***Abstract*—A novel concept for an electrically-small on-body antenna targeted for 2.4 GHz ISM band custom in-the-ear (ITE) hearing instrument (HI) applications is introduced. The antenna is based upon a cavity-backed design in order to take advantage of the maximum volume available in the ear while providing isolation from the user's body, and it occupies only 40% of the volume of the sphere with radius a = 12 mm. The antenna is implemented on a realistic 3D-printed lossy substrate and exhibits high efficiency of 70% and 22%, and a 6-dB impedance bandwidth of 108 MHz and 149 MHz, when the antenna is measured in free space and ITE, respectively. A measurement campaign conducted in free space and on a specific anthropomorphic mannequin (SAM) head with ears shows that the radiation pattern is optimal for HI applications. Furthermore, the antenna is primarily polarized normal to the surface of the head to ensure the best on-body path gain. This is substantiated by the study of the ear-to-ear (E2E) path gain, which is measured and compared to analytic and numerical results.**

***Index Terms*—Cavity-backed antennas (CBA); conformal antennas; electrically small antennas (ESA); medical devices; on-body communications; wearable antennas; wireless body-area networks (WBAN).**

I. Introduction

WEARABLE antennas for body-area network (BAN) implementation are quickly emerging as one of the major antenna application fields, drawing interest from both academia and industry. Among the different on-body communication applications, the hearing instrument (HI) industry is particularly interested in developing connectivity solutions. In fact, radio connectivity between HIs allows for advanced binaural signal processing when the important ear-to-ear (E2E) link is ensured [1]. Furthermore, the HIs may be connected to a plethora of accessories, that can be either body-worn or placed in the user's proximity, and hence to the internet as part of the so-called internet of things (IoT).

The 2.4 GHz industrial, scientific, and medical (ISM) band is preferred for this purpose due to the presence of many harmonized standards for low-power communications (such as BLE or ZigBee), its worldwide availability for industrial use, and the trade-off between power consumption and range that can be achieved. In order to ensure the connectivity of HIs, a thorough understanding of the on-body propagation mechanism of electromagnetic waves around a user's head and body is required. In particular, it is challenging but of key importance to ensure a stable E2E link: this has been the focus of much research work in recent times [2]–[7]. As the analysis of this link through software FEM solvers is extremely time consuming due to the electrical size and complexity of the models involved, an accurate channel model has been proposed [2]. This model is based on a thorough investigation of the way that creeping waves propagate around the head, and it allows to compute the E2E path gain PG in a fast and accurate manner. The proposed model is then used to compute the optimal radiation pattern for E2E communication by the use of a genetic algorithm. Additionally, it is used to estimate the variance of the E2E link, which arises due to the difference in shape among human heads, by the use of a Monte Carlo analysis [2].

The E2E link is particularly demanding in terms of requirements on the wearable antenna design and performance. In fact, in order to achieve a good on-body performance, the antenna needs to exhibit optimal radiation efficiency, bandwidth, polarization, and radiation pattern [3], while the volume available for the design is extremely reduced—as most times space comes at a premium in wearable devices. Furthermore, mass production and industrial design needs demand the antenna to be as well low-profile, lightweight, and inexpensive to manufacture. In particular, the antenna polarization characteristic is a performance parameter of utmost importance [4], but the overall constrains are many more. In fact, the efficiency may be seriously jeopardized by the proximity of the antenna to the human head, as the body tissues have very high losses around 2.4 GHz due to the high water content [8]. This may critically impact the overall performance given the magnitude of the drop in efficiency and the fact that the HI radios operate in ultra-low-power regime. Another issue threatening the antenna efficiency is the little volume available for the design, as this necessarily brings the antenna in close physical (hence, electrical as well) proximity of other parts of the device, with a strong likelihood of coupling to them [9]. A large bandwidth is as well hard to achieve for an electrically small antenna (ESA), due to its fundamental limits [10]. In this application, the bandwidth shall cover at least the whole 2.4 GHz ISM band, but a larger bandwidth would help to compensate for the detuning of the antenna caused by the body, which varies across users [11].

Most of the works that study on-body propagation makes use of simple antenna structures, in particular monopoles or general antenna designs that do not take into account the actual application needs. Some work has been done in recent time to propose antennas that are suitable for implementation in HIs, including among others a spiral monopole [12], a

Andrea Ruaro and Jesper Thaysen are with GN ReSound A/S, Lautrupbjerg 7, DK-2750 Ballerup, Denmark (e-mail: aruaro@gnresound.com, jtahysen@gnresound.com).

Kaj B. Jakobsen is with the Department of Electrical Engineering, Electromagnetic Systems, Technical University of Denmark, Ørsteds Plads, Building 348, DK-2800 Kgs. Lyngby, Denmark (e-mail: kbj@elektro.dtu.dk).

This article has been accepted for publication in a future issue of this journal, but has not been fully edited. Content may change prior to final publication. Citation information: DOI 10.1109/TAP.2016.2543800, IEEE Transactions on Antennas and Propagation

TABLE I
OVERVIEW OF THE KEY PERFORMANCE METRICS FOR HI ANTENNAS

reference	type	BW (MHz)	η_{tot} (%)	$\mathbf{P}$	a (mm)	ε_{r}	$\tan\delta$	PG_{E2E} (dB)
[12]	BTE	80^*	—	$\parallel$	5	1.1	0.000	-80
[13]	ITE	76	5.3	$\perp$	10^*	6.0	0.002	-73^*
[14]	ITE	10^*	0.3^*	$\perp^*$	7^*	3.6	0.003	-89^*
[15]	BTE	240^*	—	$\perp$	11	1.1	0.000	-50
This work	ITE	149	22	$\perp$	12	2.4	0.012	-63

'*' denotes different observation conditions.

slot loop [13], a wire-patch [14], and a balanced PIFA [15]. Nevertheless, none fully characterizes the antenna performance measuring all the performance metrics mentioned above. In fact, a measure of the reflection coefficient alone is not sufficient, as most of the energy accepted by the antenna is dissipated in the head in form of heat [8]. Instead, the E2E path gain measure is an excellent performance metric, but on the other side it is a system-level measurement affected by multiple factors and typically needs to be substantiated by numerical results. An overview of the key performance metrics for the mentioned designs is reported in Table I. From left to right are shown in the table, respectively: the reference source; the position of the antenna on the head, either behind-the-ear (BTE) or in-the-ear (ITE); the bandwidth BW; the total radiation efficiency η_{tot}; the main direction of the polarization vector $\mathbf{P}$ (either tangential $\parallel$ or normal $\perp$ to the head surface) [16]; the radius a of the minimum sphere encompassing the antenna; the dielectric constant ε_{r} and the loss tangent $\tan\delta$ of the support substrate; and the maximum E2E path gain PG_{E2E}. All data applies to the 2.4 GHz ISM band. Where available, measured data are preferred to simulation results. The data marked with an asterisk (*) are either strongly dependent on the specific context, or approximated, or non-uniquely defined, or selected among multiple options available in the source: the reader is encouraged to look up the original reference in order to understand the reported data.

On the other hand, cavity-backed antennas were studied in details well in the past, but they were not used for on-body applications until very recent times [16]–[19]. One of the main advantages of cavity-backed antenna is that they are not significantly affected by the electronic environment around them, as the cavity provides some sort of electromagnetic shielding. Based upon this principle only, even without an optimal current distribution, an interesting on-body performance can be achieved by a large, early-stage prototype, where the cavity does not actively contribute to the radiation mechanism [19]. This work introduces and fully characterizes a novel wearable shell antenna based on an open cavity-backed design. The very shell of a customized in-the-ear (ITE) HI is used as part of the antenna. The design is detailed and a prototype is fully characterized by means of numerical simulations and measurements. Selective Heat Synthering (SHS) 3D-printed plastics are used for the antenna frame. This process has been recently characterized at radio frequencies and it allows for an accurate numerical modeling [20].

The article is organized as follows. Section II describes the theoretical principles, the design and the implementation of the antenna. Section III presents the measurement set-up and results, and discusses them. Section IV analyzes the performance of the antenna along the critical ear-to-ear path. Finally, Section V summarizes the findings.

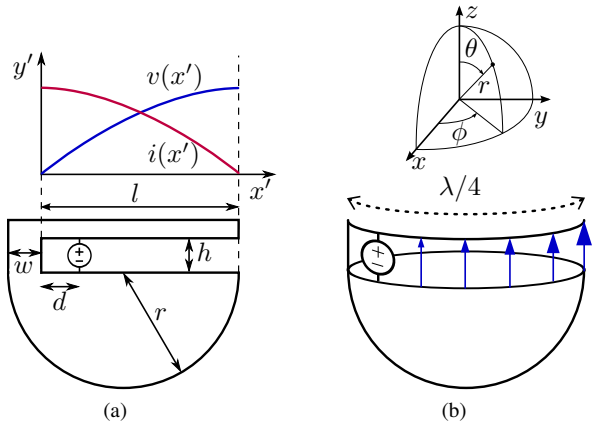

Fig. 1. Antenna diagram, (a) profile and (b) 3D view.

II. THEORY AND DESIGN

A novel antenna is proposed based on the geometry shown in Fig. 1 in order to address all the complex requirements that the hearing instrument application demands.

Simple equations of the radiated fields are not trivial to derive from the field distribution in the aperture. While closed-form expressions exist both for a slot antenna, which can be analyzed as the dual of the equivalent flat wire antenna [16], or an antenna fully backed by a cavity [17], factors like the conformal shape, the small ground plane and the position of the antenna at its edge, and the curvature of the antenna arm, makes it unrealistic to derive a simple equation-based model. The principle of how the antenna function is hence best understood via analogy to an Inverted F-Antenna (IFA) or an open-ended $\lambda/4$ slot antenna. If the antenna cavity is loaded with a dielectric material, the wavelength is $\lambda = \lambda_0/\sqrt{\varepsilon_{\mathrm{eff}}}$, where λ_0 is the free space wavelength and $\varepsilon_{\mathrm{eff}}$ the effective dielectric constant at the substrate–air interface. For the purpose of symmetry, consider a hemispherical ground plane of radius r, with the edge laying in the xy-plane. A wire is electrically connected to the ground plane, bent at a height h, and curved to follow the edge of the hemispherical cavity. The distance between the wire and the edge of the ground plane is kept

This article has been accepted for publication in a future issue of this journal, but has not been fully edited. Content may change prior to final publication. Citation information: DOI 10.1109/TAP.2016.2543800, IEEE Transactions on Antennas and Propagation

constant at h. The length of the wire is such that the current has an antisymmetric distribution around the slot of length l, i.e.,

$$l = \frac{\lambda/2 + h}{2} \approx \lambda/4 \text{ for } h \ll \lambda \ . \quad (1)$$

Please note, this is somewhat independent on the radius r of the hemispherical ground plane, when it respects the condition:

$$2\pi r > l \Leftrightarrow r > \lambda/8\pi \ . \quad (2)$$

The antenna radiation mechanism is best understood when the voltage distribution shown in Fig. 1 is considered. In fact, the current at the end of the antenna arm is null. As the distance from the open end to the short-circuiting pin is $\lambda/4$, the current distribution is sinusoidal and reaches a maximum at the pin. The pin width w is chosen large enough in order not to present a significant self-inductance at the operating frequency. The voltage distribution is 90° out of phase with respect to the current: therefore, at the short-circuiting pin the voltage across the slot is null, while it reaches a maximum at the open end. The feed structure excites a voltage across the slot. Even though the impedance across the slot varies in a complex way as discussed above [17], it is very high at the open end and very low at the short-circuiting pin. As the impedance increases monotonically, there exists a $50\ \Omega$ matched point that can be found at a distance d from the short-circuiting pin.

As the antenna is meant to fit in the ear, it has to be modeled according to each user's unique ear canal shape. The design process starts from this specific physical form, and therefore it is necessary to abandon the symmetry of the cavity and replace it with a more realistic model as shown in Fig. 2. In the hearing industry, this is typically done by taking an impression of the external auditory canal and of the concha. Here, the software model shown in Fig. 2 is generated from a given ear shape. The antenna is then built on a 3D-printed plastic substrate to fit the custom shape of the designed specific anthropomorphic mannequin (SAM) ear. The support is realized with a Selective Heat Synthering (SHS) process that exhibits a dielectric constant $\varepsilon_\mathrm{r} = 2.4$ and a loss tangent $\tan\delta = 0.0012$ at the frequency of interest [20]. The conductive layers, i.e., the ground plane and the antenna arm, are implemented with solid copper. A picture of the right ear prototype is shown in Fig. 2d. The final design parameters are based on the idealized model described above, and are optimized for the ITE performance in a commercial FEM software simulator. The shape of the custom cavity, as given by the ear model, and h were assumed as given working assumptions, whereas l, w, and d were subsequently optimized with respect to center frequency and bandwidth. Since the realistic cavity shape is not hemispherical as in the idealized model, the parameter r is undefined. In order to discuss the antenna physical and electrical size, it is therefore replaced by the radius a of the minimum sphere encompassing the antenna. The design parameters of the antenna are listed in Table II.

In order to maximize the on-body performance, the antenna has to have high radiation efficiency, be polarized normally to the head surface, have a omnidirectional radiation pattern in the plane tangential to the head, and have a sufficient

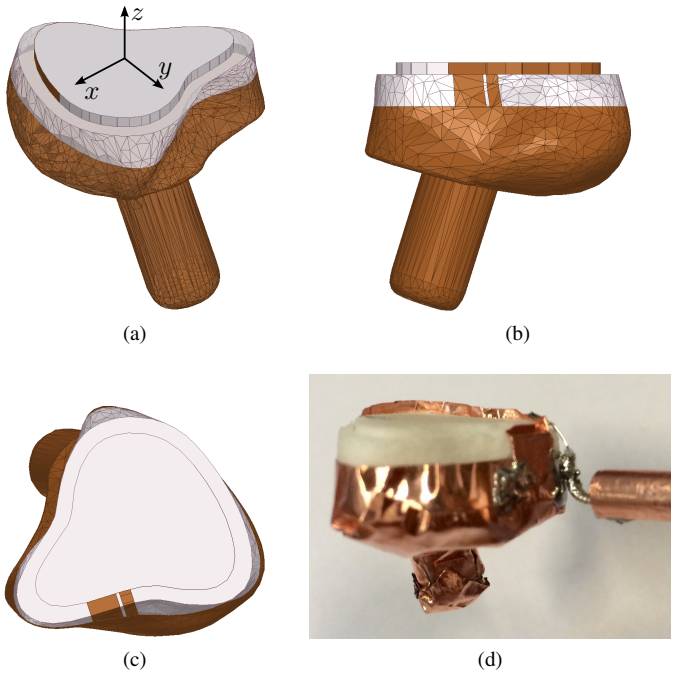

Fig. 2. Custom shell antenna: (a–c) CAD model, different views; (d) picture of the prototype.

TABLE II
ANTENNA DESIGN PARAMETERS

l	23.5 mm
h	2.7 mm
w	2.6 mm
d	0.5 mm
a	12.0 mm
ka	0.62 rad
ε_r	2.4
$\tan\delta$	0.012

impedance bandwidth [3]. The efficiency requirement is determined by the fact that the power that is absorbed into the head is, in fact, dissipated in form of heat. Without even addressing the regulatory issues, this translates in practical applications in a drastic drop of the antenna efficiency. A good way to minimize this is to effectively use the antenna part farther away from the head to concentrate the **E**-field. An antenna with a small ground plane has higher losses given the spatial distribution of its reactive near field [3]. The ground plane helps in shielding the head from the radiation, in a similar way to the widespread use of the ground plane in PIFAs in order to reduce the backward radiation [8].

The radiation pattern on the plane tangential to the body surface and the polarization characteristics are of key importance in order to properly excite strong surface waves. In fact, the signal level in the line-of-sight (LOS) scenario is enough for most applications once sufficient radiation efficiency is guaranteed, as there is no body shadowing—on the contrary, the body can partly act as a reflector [21]. Instead, when the receiving antenna is placed in non-line-of-sight (NLOS), these parameters acquire critical importance. The polarization is the

This article has been accepted for publication in a future issue of this journal, but has not been fully edited. Content may change prior to final publication. Citation information: DOI 10.1109/TAP.2016.2543800, IEEE Transactions on Antennas and Propagation

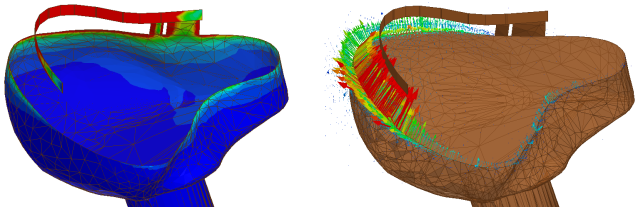

(a) (b)

Fig. 3. Plot of the antenna with overlaid (a) current magnitude and (b) **E**-field vector.

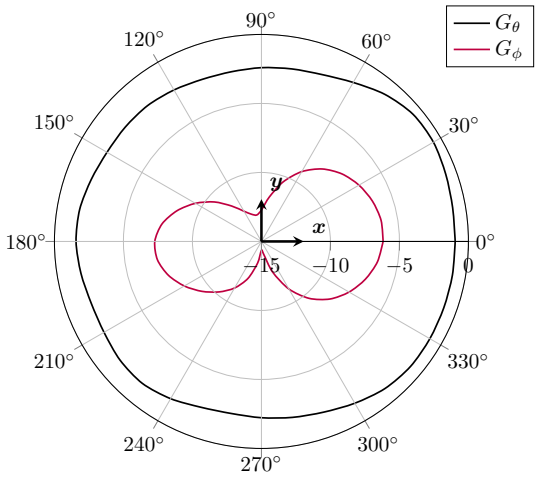

Fig. 4. Simulated free space antenna gain in the xy-plane, divided into its polarization components G_θ and G_ϕ.

dual of that of a flat wire; hence it is normal to the head surface. This can also be seen by the distribution of the surface current and of the **E**-field shown in Fig. 3. This is optimal in order to excite a strong surface wave along the body [3]. Please note that the polarization is weakly dependent on the radius of curvature of the antenna arm, and therefore is suitable to conform to different ear morphologies.

The radiation pattern is optimal as well, as can be seen by the plot of the θ- and ϕ-component of the simulated free-space antenna gain plotted in Fig. 4. There is a strong dominance (above 6 dB in every direction) of the θ-component over the ϕ-component on the plane tangential to the head surface.

The bandwidth is optimized by the shape of the ground plane. In fact, an IFA is strongly dependent on the ground plane dimensions, which impacts the polarization of its main radiation mode and has to be electrically large. A decrease in the size of the ground plane beyond a certain limit may seriously jeopardize the performance of an IFA [22]. Therefore, it is important to maximize the ground plane size within the volume at disposal. In this case, the hemispherical shape maximizes the available volume within half of the Wheeler's sphere [23] and uses most of the available surface to implement the ground plane. This lowers the Q factor, i.e., it results in a larger bandwidth [10]. The electrical size ka of the antenna is promptly obtained in the simplified geometry, as the radius a of the sphere circumscribing the antenna is

$$a = \sqrt{r^2 + h^2} \approx r \text{ for } h \ll r \ , \tag{3}$$

whereas for the custom shaped antenna the actual value reads $ka = 0.62$ rad at a frequency $f = 2.45$ GHz. In the idealized case, the antenna uses only approximately 50% of the volume of the circumscribing sphere. The custom shaped antenna uses only 40% of the volume of the sphere of radius $a = 12$ mm. Even though the shell antenna shape is conformal to the ear canal, the currents are confined in the area close to the aperture: therefore, the design is less dependent upon the specific shape of a given ear. The idealized model works well in this sense. Another advantage of this architecture is that it is relatively insensitive to the presence of conductive parts within the shell itself, e.g., a battery or a device's electronics [24]. Electromagnetic coupling to other parts of a device, which include among others loudspeaker's coils, can easily worsen the radiation efficiency of the antenna [9].

III. Measurement Results

A. Set-up

The designed antenna prototype was measured in free space (FS), as a reference, and on-body. The on-body measurements are conducted with the antenna placed in-the-ear (ITE) of a SAM head. The shape of the antenna shell is designed to fit such ear design. The ear material is a CTIA-compliant [25] homogeneous silicone-carbon dielectric with average electrical properties $\varepsilon_{\mathrm{r,ear}} = 28$ and $\sigma_{\mathrm{ear}} = 1.15$ S/m at $f = 2.45$ GHz (data measured by the supplier). The low-loss outer shell of the SAM head itself is 2 mm thick. This was not included in the simulation set-up, where a homogeneous head model is used. This was shown to possibly influence the measured results [5], but as shown below, it is not deemed critical here. The fill liquid in the phantom is targeted to $f = 2.4$ GHz and is CTIA compliant [25], with nominal electrical properties $\varepsilon_{\mathrm{r,SAM}} = 44$ and $\sigma_{\mathrm{SAM}} = 2$ S/m. The slight difference in the electrical properties between the CTIA-compliant liquid and the FEM model is neglectable [2].

The antenna is fed with a coaxial cable. The VNA measurements used the port extension correction in order to measure the S-parameters, including the phase, at the true antenna port. To prevent the RF cable to radiate as a consequence of the spurious currents running on it, as the antenna has an unbalanced architecture, a $\lambda/4$ bazooka balun is soldered onto the cable itself as visible in Fig. 2d. The cable hence does not represent an extension of the small ground plane, and the presence of spurious currents running on the coaxial cable outer shell was not observed during the analysis at the VNA. In any case, during the measurements the cable lays onto a plane tangential to the head, so that it is mostly ϕ-polarized (as it is a wire radiator) to ensure an even lesser impact on the measurement results.

The measurement campaign was conducted in a ETS-Lindgren commercial anechoic chamber. The measurement coordinate system is shown in Fig. 2 for the antenna in free space, and in Fig. 5 for the antenna placed in-the-ear of the SAM head. In free space, the antenna arm lays on the xy-plane, with the positive z-axis oriented toward the opposite side of the conductive shell. The origin of the coordinate system is centered with respect to the center of the

This article has been accepted for publication in a future issue of this journal, but has not been fully edited. Content may change prior to final publication. Citation information: DOI 10.1109/TAP.2016.2543800, IEEE Transactions on Antennas and Propagation

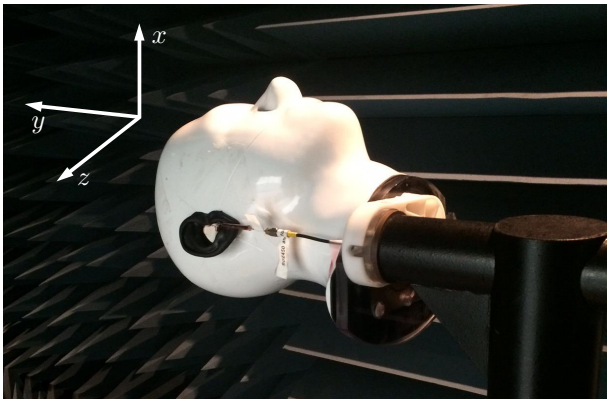

Fig. 5. Picture of the measurement set-up, with the antenna coordinate system.

circle circumscribing the antenna on the xy-plane. The same orientation is kept when the antenna is measured on the head, i.e., the xy-plane is the plane tangential to the head surface and the z-axis is normal to the head surface. The origin of the coordinate system is centered at the right ear of the SAM. The measurements are reported for the right ear prototype.

In the anechoic chamber, ferrite beads were mounted on the feed cable to the antenna connector in order to suppress spurious radiation. The distance of the antenna from the mast that controls the rotation is 250 mm, i.e., approximately $2\lambda_0$ at the operating frequency $f = 2.4$ GHz. Some reflections and shadowing in the radiation patterns are due the presence of the mast. The measured fields are directly sampled in the Fraunhofer region, and are therefore considered a good approximation of the true far field. The chamber is calibrated. The data are processed by the chamber manufacturer's proprietary software EMQuest$^{\text{TM}}$ EMQ-100. The total efficiency is computed based on the estimation of the total radiated power (TRP) of the antenna.

For the in-the-ear measurements, the antenna is fitted within the SAM ear as shown in Fig. 6b and Fig. 6d, whereas the ear canal works as a guide. The semielastic dielectric material, which the ears are made of, introduces a small air gap in between the antenna and the ear surface. It can be seen from Fig. 6a and Fig. 6c how the profile of the antenna is low on the ear, as it is meant to be operated in the case of hearing instruments. The antenna feed sits in between the tragus and the anti-tragus, with the end of the antenna arm fitted in the concha. In this area, which is where the antenna is farther from the tissue, is where the concentration of the $\mathbf{E}$-field is highest. The feed cable descends in front of the lobule toward the neck. It is of interest to notice that in this way the position of the antenna feed in the shown prototype differs from that used in the software optimization. This variation does not introduce a significant change in the current distribution or in the measured radiation performance shown, e.g., in Fig. 8. This is due to the fact that the current magnitude is low on most of the shell surface as shown in Fig. 3a, and therefore the rotational shift of the feed does not noticeably impact the currents running on the edge of the shell, which occur in proximity of the antenna arm.

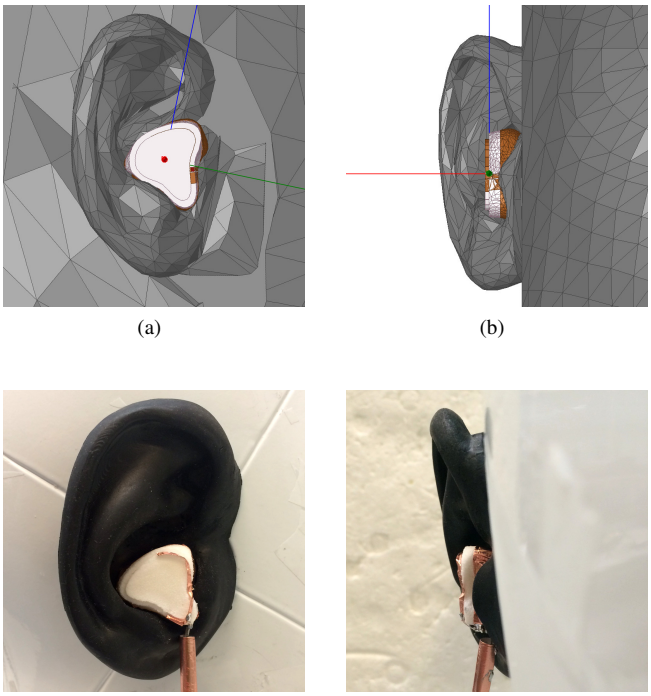

(a) (b) (c) (d)

Fig. 6. Detail of the antenna fitted into the human ear. Position in the FEM solver, (a) front view and (b) side view, and position in the SAM ear, (c) front view and (d) side view.

B. Results

There is a rather strong general agreement between measurements and simulations. From the voltage standing wave ratio $VSWR$ shown in Fig. 7, it is seen how the impedance match improves and becomes significantly more wideband when the antenna is worn. This is expected, as it means that a significant amount of the power is not being reflected back to the VNA: hence it might be radiated, or dissipated in form of losses in the antenna dielectric fill or in the human tissues.The antenna is de-tuned when worn, as a consequence of the capacitive loading provided by the proximity of the human body. This is seen in both simulations and measurements. The impedance match was chosen to optimize the antenna performance in the ITE case. The bandwidth performance of the antenna is rather remarkable given its overall dimensions. The bandwidth is defined here as the impedance bandwidth for $|S_{11}| \leq -6$ dB, or equivalently $VSWR \leq 3$. In fact, as bandwidth is not uniquely defined, this is a commonly accepted value given the application, in addition to the fact that the antenna is severely space-constrained [26]. The measured free space impedance bandwidth is $BW_{6\text{dB,FS}} = 108$ MHz $\sim 4.4\%$, and the on-body bandwidth is $BW_{6\text{dB,ITE}} = 149$ MHz $\sim 6.1\%$. The performance is comparable to that of an IFA on a large solid ground plane in the 2.4 GHz band [27], whereas the arm height here is 2.7 mm only.

The simulated and measured radiation efficiency is plotted if Fig. 8. The free space efficiency is excellent, especially recalling the high dielectric loss tangent of the mechanical support. It peaks at -1.54 dB $\sim 70\%$ for a frequency $f = 2.51$ GHz. The on-body efficiency peaks at -6.50 dB $\sim 22\%$ at

This article has been accepted for publication in a future issue of this journal, but has not been fully edited. Content may change prior to final publication. Citation information: DOI 10.1109/TAP.2016.2543800, IEEE Transactions on Antennas and Propagation

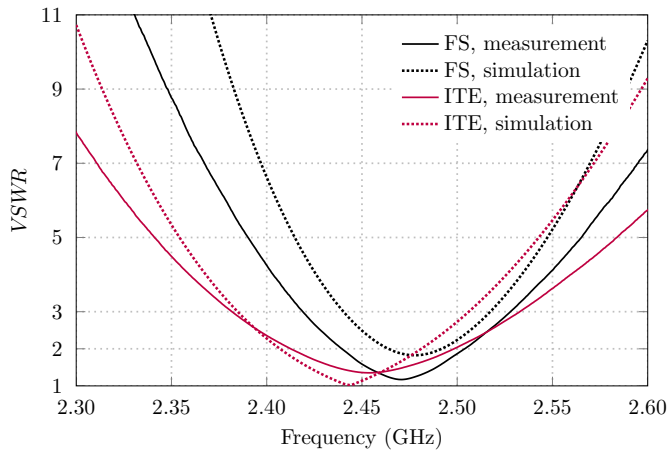

Fig. 7. The reflection coefficient expressed as $VSWR$ at the antenna interface in free space (FS) and on the SAM head in-the-ear (ITE).

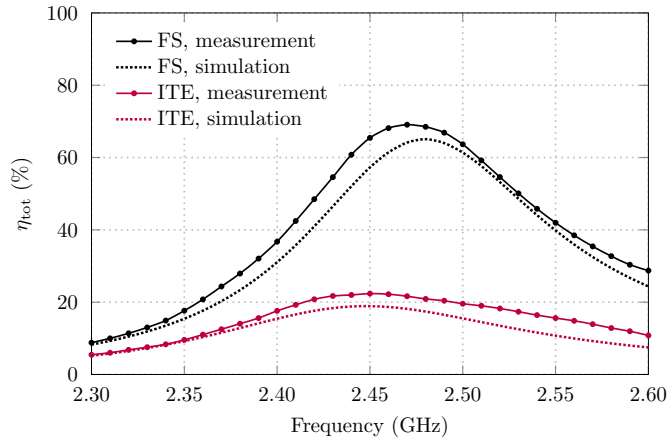

Fig. 8. The antenna radiation efficiency in free space (FS) and on the SAM head in-the-ear (ITE).

$f = 2.45$ GHz, while in the whole 2.4 GHz ISM band it is above -7.54 dB. The efficiency drop is around 5 dB only. This is deemed rather reasonable for a wearable antenna inserted deep in the body, and is due to the shielding effect provided by the conformal ground plane among other factors.

With regards to specific absorption rate (SAR) assessment, it shall be noted that due to the very low power of the related applications, no SAR study is required by regulatory bodies [28]. In fact, wearable devices are required to operate as low-power applications in order to preserve the battery's lifetime. Therefore, the value of the radiated fields is typically several orders of magnitude smaller than that of, e.g., handset applications. In the case of an example HI, the peak output power of the radio chip may be in the few-mW range; furthermore, the radio operates with low duty cycle, i.e., below 5% [29]. Therefore, as SAR is a system metric, the average output power $P_{\text{out}} = 0.05$ mW $= -13$ dBm is used in this case for SAR calculations [30], [31]. The devices are well below the SAR test exclusion threshold due to the extremely low power operation [28]. The SAR values are shown for different average output power P_{out} values in Table III. The values are numerically simulated with Ansys HFSS™ and are estimated

TABLE III
SAR VALUES

P_{out} (dBm)	$\text{SAR}_{1\text{g}}$ (W/Kg)	$\text{SAR}_{10\text{g}}$ (W/Kg)
-13	$7 \cdot 10^{-3}$	$2 \cdot 10^{-4}$
0	0.13	0.04
10	1.30	0.35

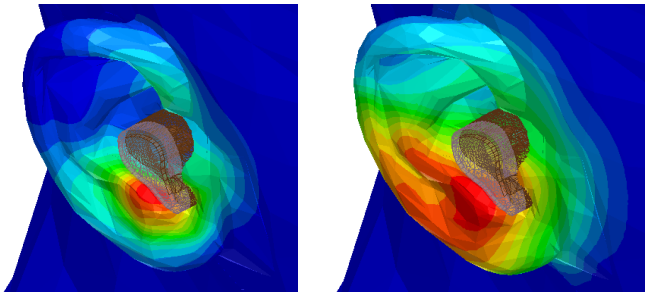

(a) (b)

Fig. 9. Spatial distribution of the SAR value, averaged over (a) 1 g (FCC) and (b) 10 g (IEC) of tissue, normalized to the relative peak value listed in Table III, respectively. The color scale ranges from blue (minimum) to red (maximum).

conservatively. While the first reported case is representative of actual HI operation, the second ($P_{\text{out}} = 1$ mW $= 0$ dBm) refers to potential continuous-wave operation, or operation with a duty cycle of 100%, equivalently. The third case listed in Table III is the limit case for BTLE operation (within the ETSI range) [29] with 100% duty cycle, and still falls below the regulatory limits. Fig. 9 shows the SAR spatial distribution normalized to each case peak value, respectively.

The radiation patterns for the antenna are shown in Fig. 10 and Fig. 11 for the free space and on-body case, respectively. The respective coordinate systems are those shown in Fig. 2 and Fig. 5, respectively, with the open side of the cavity oriented toward positive z-axis and the xy-plane being tangential to the head. In free space, the antenna is nearly omnidirectional in the xy-plane as desired. The tilt on the yz-cut is mostly dependent on the inclination of the **E**-field. In fact, in Fig. 3b it can be seen that the **E**-field is not purely z-aligned since the antenna arm is inset slightly inwards. In the measurements, the back lobe is affected by the presence of the chamber mast. This introduces some reflections and generates an angle-dependent ripple. The omnidirectionality in the xy-plane is maintained when the antenna is fitted into the SAM ear. In the xz- and yz-cuts the head shadowing effect can be observed. Overall, there is a reasonably good agreement between the simulated and measured radiation patterns that are shown in Fig. 10 and Fig. 11, especially taking into account the the differences between the software model and the actual prototype, and the repeatability of the antenna placement in the real life scenario.

The performance of the antenna is summarized in Table IV for the FS and ITE cases.

This article has been accepted for publication in a future issue of this journal, but has not been fully edited. Content may change prior to final publication. Citation information: DOI 10.1109/TAP.2016.2543800, IEEE Transactions on Antennas and Propagation

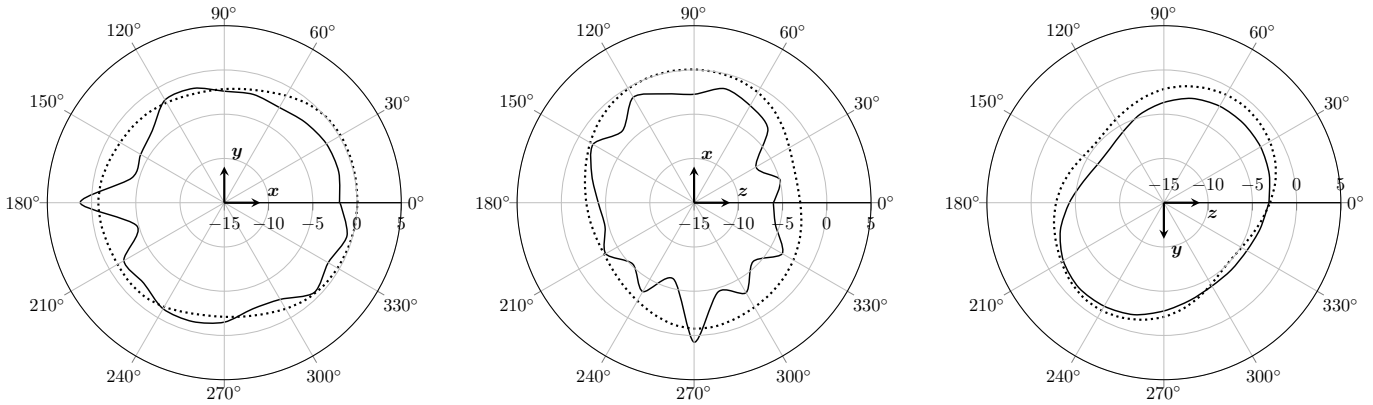

Fig. 10. Free space radiation patterns (antenna total gain) in dBi, measured (solid line) and simulated (dotted line). Left: xy-plane ($\theta = 90°$). Center: E-plane ($\phi = 0°$). Right: H-plane ($\phi = 90°$). The patterns are plotted at $f = 2.45$ GHz.

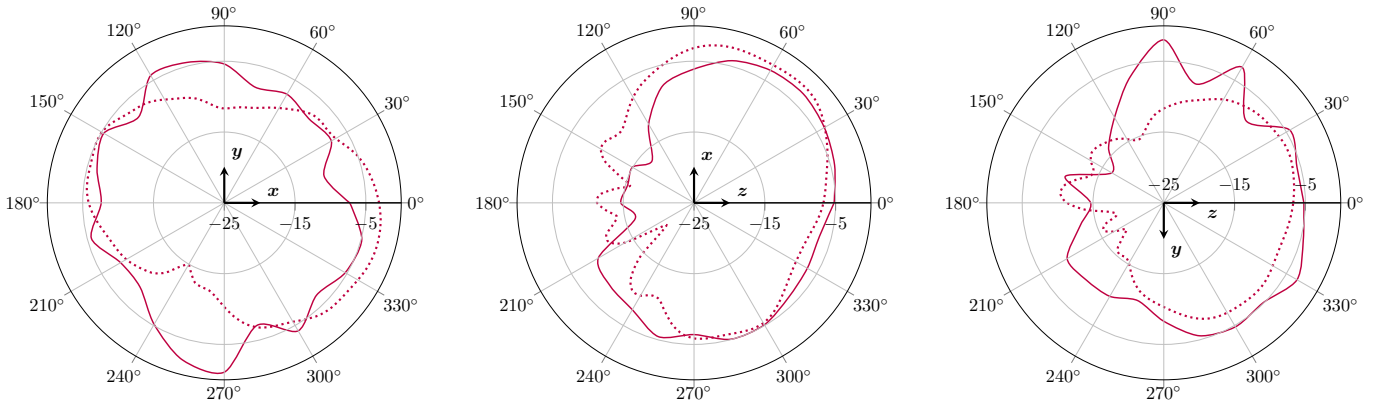

Fig. 11. In-the-ear radiation patterns (antenna total gain) in dBi, measured (solid line) and simulated (dotted line). Left: xy-plane ($\theta = 90°$). Center: E-plane ($\phi = 0°$). Right: H-plane ($\phi = 90°$). The patterns are plotted at $f = 2.45$ GHz.

TABLE IV
MEASURED ANTENNA PERFORMANCE

	FS	ITE	
$BW_{6\text{dB}}$	108	149	MHz
η_{peak}	-1.54	-6.50	dB
$PG_{\text{E2E,avg}}$	—	-66.1	dB

IV. EAR-TO-EAR LINK

In order to achieve binaural hearing benefits as mentioned in the introduction, each hearing instrument need to be able to communicate with another one that is placed at the opposite side of the head [1]. In this sense, the Ear-to-Ear (E2E) connectivity is the key parameter that has to be ensured by the antenna design. This is dependent upon the antenna radiation properties, such as efficiency and polarization, and on the path loss along the surface of the head. The overall loss is high since most of the electromagnetic energy is radiated directly into the space along the LOS directions, whereas the NLOS propagation around the head has to rely on creeping waves.

As anticipated in the introduction, Kvist *et al.* [2] recently proposed a method to calculate the E2E path gain PG using creeping waves along a number of elliptical paths around the head. This approach draws a series of elliptical paths with different semi-major axes to reproduce the shape of the head, where the convergence of the path gain is obtained for a sufficiently high number of paths. The radiation pattern of the antenna is then taken into account as a weight function in order to provide the excitation along these paths, each one representing a separate creeping wave that propagates around the head.

This result is compared to numerical simulation results obtained by a commercial FEM solver. Also in this case, the convergence of the simulation is reached to ensure a reasonable uncertainty on the very low path gain level. PMLs layer are places around the truncated human body model to absorb incident radiation and to avoid a non-physical contribution from the propagation of electromagnetic waves along these boundaries.

For the E2E path gain measurements, the same SAM head that was detailed in Section III was used with the set-up shown in Fig. 12. A VNA was used to record the path gain $|S_{21}|$. The measurements were conducted in a shielded chamber with EM absorbers. The cables were routed as far as possible from each other to avoid coupling in between them. Both the VNA and the operator were shielded as much as possible by absorbers. Signal averaging was used to minimize the impact of the reflections from the operator.

The measured E2E path gain agrees well with the analytic

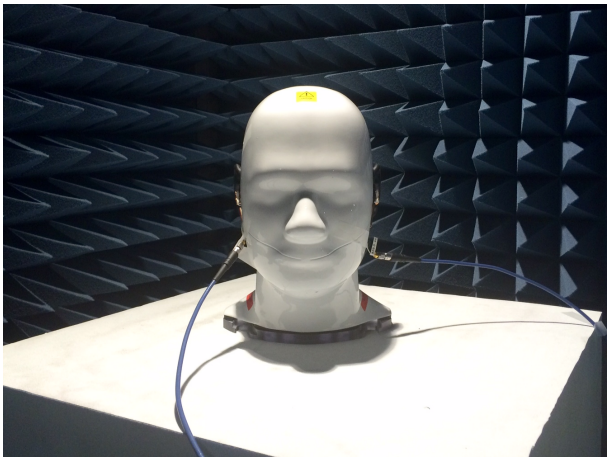

Fig. 12. Picture of the set-up for the measurement of the E2E path gain.

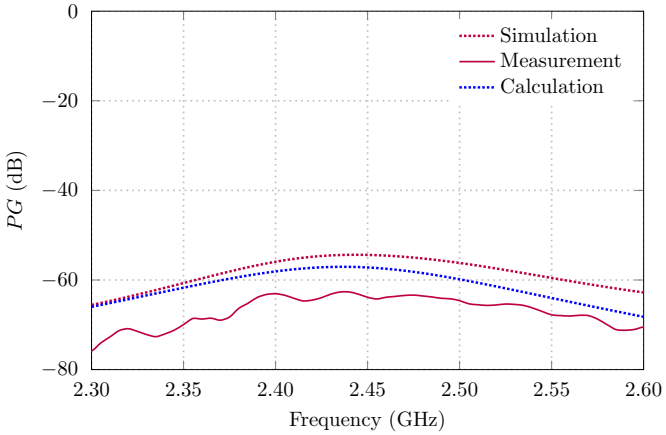

Fig. 13. Plot of the E2E Path Gain (PG), with results from FEM simulation, measurements on SAM head, and calculation based on the analytic model [2].

and numerical calculations, and with previous studies reported by multiple authors [2], [3], [5]–[7], [12]–[15]. The results are shown in Fig. 13. It can be seen that the strong θ-component excited by the antenna assists in ensuring a good E2E path gain, with a simulated maximum of $PG_{\mathrm{sim}} = -54.4$ dB at a frequency $f = 2.44$ GHz. The calculated model falls close, with an absolute difference from the simulated value of only $\Delta PG = PG_{\mathrm{sim}} - PG_{\mathrm{calc}} = 0.05\%$ at a frequency $f = 2.44$ GHz. The deviation of the model from the simulated result increases with frequency as the propagation paths become electrically longer. This suggests a possible influence of the undefined antenna phase center. In fact, given its configuration, when placed on-body the antenna does not possess a clearly identifiable phase center. The difference in the electrical length of the propagation paths may also be the cause for the lower E2E path gain that was measured, as the antenna was placed on the SAM slightly below the position that was used for the simulation, as can be seen in Fig. 6.

V. Conclusion

A novel wearable shell antenna was introduced in this work. The application as an on-body hearing instrument antenna was studied. In particular, the novel concept makes use of a ground plane conformal to a user's ear canal to maximize the available volume and reduce the losses caused by the human body, while it ensures high radiation efficiency and a strong polarization component normal to the head surface. The operating principle of the antenna was analyzed by means of analogies to the well-known radiating mechanism of IFAs and slot antennas. The antenna has been fully characterized with the study of the reflection coefficient and matching, radiation efficiency, simulated currents and fields, and radiation pattern, both in free space and when worn in-the-ear (ITE). Furthermore, the critical parameter E2E path gain was studied and compared to a deterministic model that showed a convergence among computation, FEM simulation, and measurements.

References

[1] B. C. Kirkwood, S. A. Hallenbeck, and T. Stender, "How can wireless data exchange in hearing instruments contribute to binaural hearing?" *Hearing Review*, vol. 19, no. 10, pp. 52–55, 2012.

[2] S. Kvist, J. Thaysen, and K. Jakobsen, "Ear-to-ear on-body channel model for hearing aid applications," *IEEE Trans. Antennas Propag.*, vol. 63, no. 1, pp. 344–352, Jan. 2015.

[3] P. S. Hall *et al.*, "Antennas and propagation for on-body communication systems," *IEEE Antennas Propag. Mag.*, vol. 49, no. 3, pp. 41–58, 2007.

[4] N. P. I. Kammersgaard, S. H. Kvist, S. Özden, J. Thaysen, and K. B. Jakobsen, "Body-worn antennas for body-centric wireless communications," in *Loughborough Antennas Propag. Conf. (LAPC)*, 2014.

[5] R. Chandra and A. J. Johansson, "A link loss model for the on-body propagation channel for binaural hearing aids," *IEEE Trans. Antennas Propag.*, vol. 61, no. 12, pp. 6180–6190, 2013.

[6] S. H. Kvist, S. Özden, J. Thaysen, and K. B. Jakobsen, "Improvement of the ear-to-ear path gain at 2.45 GHz using parasitic antenna element," in *Proc. of 6th European Conf. Antennas Propag. (EuCAP)*, vol. 2, 2011, pp. 944–947.

[7] A. Vasylchenko, C. Hennemann, and R. Dubrovka, "Characterization of the ear-to-ear propagation channel using microstrip dipole antennas," in *Proc. 8th Int. Conf. Antenna Theory Techn. (ICATT)*, 2011, pp. 202–204.

[8] M. Jensen and Y. Rahmat-Samii, "EM interaction of handset antennas and a human in personal communications," *Proc. IEEE*, vol. 83, no. 1, pp. 7–17, 1995.

[9] X. Chen, N. Chavannes, G. Ng, Y. Tay, and J. Mosig, "Analysis and design of mobile device antenna–speaker integration for optimum over-the-air performance," *IEEE Antennas Propag. Mag.*, vol. 57, no. 1, pp. 97–109, Feb 2015.

[10] A. D. Yaghjian and S. R. Best, "Impedance, bandwidth, and Q of antennas," *IEEE Trans. Antennas Propag.*, vol. 53, no. 4, pp. 1298–1324, 2005.

[11] S. Pehrson, S. H. Kvist, K. B. Jakobsen, and J. Thaysen, "Morphological investigation of the differences on the ear-to-ear path gain and the packet loss at 2.45 GHz," *34th Annu. Antenna Meas. Techn. Assoc. Symp. (AMTA)*, pp. 43–48, 2012.

[12] N. Kammersgaard, S. Kvist, J. Thaysen, and K. Jakobsen, "In-the-ear spiral monopole antenna for hearing instruments," *Electronics Letters*, vol. 50, no. 21, pp. 1509–1511, October 2014.

[13] W. H. Yatman, L. K. Larsen, S. H. Kvist, J. Thaysen, and K. B. Jakobsen, "In-the-ear hearing-instrument antenna for ISM-band body-centric ear-to-ear communications," in *Loughborough Antennas Propag. Conf. (LAPC)*, 2012.

[14] L. Huitema, S. Sufyar, C. Delaveaud, and R. D'Errico, "Miniature antenna effect on the ear-to-ear radio channel characteristics," in *Proc. of 6th European Conf. Antennas Propag. (EuCAP)*, 2012, pp. 3402–3406.

[15] S. H. Kvist, K. B. Jakobsen, and J. Thaysen, "Design and measurement of a 2.45 GHz on-body antenna optimized for hearing instrument applications," in *34th Annu. Antenna Meas. Techn. Assoc. Symp. (AMTA)*, 2012, pp. 33–37.

[16] C. Balanis, *Antenna theory: analysis and design*, 3rd ed. John Wiley, 2005.

[17] C. R. Cockrell, "The input admittance of the rectangular cavity-backed slot antenna," *IEEE Trans. Antennas Propag.*, vol. 24, no. 3, pp. 288–294, 1976.

[18] N. Haga, M. Takahashi, K. Saito, and K. Ito, "A cavity-backed slot antenna for on-body BAN devices," in *Proc. IEEE Int. Workshop Antenna Technol. (IWAT)*, 2008, pp. 510–513.

[19] A. Ruaro, J. Thaysen, and K. B. Jakobsen, "Cavity-backed on-body antenna for custom hearing instrument applications," *Electronics Letters*, 2015.
[20] ——, "Rapid prototyping analysis and modeling of a small antenna for binaural hearing aids," in *Int. Symp. Antennas Propag. (ISAP)*, 2015.
[21] N. P. I. Kammersgaard, S. H. Kvist, J. Thaysen, and K. B. Jakobsen, "Pinna model for hearing instrument applications," in *Loughborough Antennas Propag. Conf. (LAPC)*, 2014, pp. 141–143.
[22] M. C. Huynh and W. Stutzman, "Ground plane effects on planar inverted-F antenna (PIFA) performance," *IEE Proc. Microw. Antennas Propag.*, vol. 150, no. 4, pp. 209–213, 2003.
[23] H. Wheeler, "The radiansphere around a small antenna," *Proc. IRE*, vol. 47, no. 8, pp. 1325–1331, 1959.
[24] A. Ruaro, J. Thaysen, and K. B. Jakobsen, "Battery coupling impact on the antenna efficiency in a small wearable device," in *Loughborough Antennas Propag. Conf. (LAPC)*, 2015.
[25] CTIA Certification, "Test plan for wireless device over-the-air performance," v3.3.2, September 2014.
[26] Y. Rahmat-Samii, J. Guterman, A. A. Moreira, and C. Peixeiro, "Integrated antennas for wireless personal communications," in *Modern Antenna Handbook*, C. A. Balanis, Ed. John Wiley & Sons, Inc., 2007, pp. 1077–1142.
[27] D. Liu and B. Gaucher, "The inverted-F antenna height effects on bandwidth," in *Proc. IEEE Antennas Propag. Symp.*, vol. 2, 2005, pp. 367–370.
[28] Federal Communications Commission, "447498 D01 general RF exposure guidance," version 6, October 2015.
[29] Bluetooth SIG Regulatory Committee, "Bluetooth low energy regulatory aspects," version 10, April 2011.
[30] International Electrotechnical Commission, "Human exposure to radio frequency fields from hand-held and body-mounted wireless communication devices - Human models, instrumentation, and procedures," IEC 62209-2:2010, part 2, March 2010.
[31] IEEE International Committee on Electromagnetic Safety, "IEEE recommended practice for measurements and computations of radio frequency electromagnetic fields with respect to human exposure to such fields, 100 kHz-300 GHz," IEEE Std C95.3-2002 (R2008), December 2002.

Andrea Ruaro was born in Venezia, Italy, in 1988. He received the B.Sc. degree in Information Engineering from the University of Padova in 2010, and the M.Sc. and Ph.D. degree in Electrical Engineering from the Technical University of Denmark in 2012 and 2016, respectively. Since 2012 he has been affiliated with GN ReSound A/S, a leading hearing instrument manufacturer.

His research interests include electromagnetic interaction and coupling, EMC, and on-body antennas and propagation.

Jesper Thaysen received the B.Sc., M.Sc., and Ph.D. degrees in electrical engineering from the Technical University of Denmark in 1998, 2000 and 2005, respectively. Since 2008 he has been employed at GN ReSound A/S, a Danish hearing instrument manufacturer, where he currently acts as the Director of the Radio Systems group in R&D.

His research interests include small antennas and on-body antennas and propagation. Dr. Thaysen has overseen more than 40 B.Sc. and M.Sc. students, as well as 3 Ph.D. students, as the company representative in university-industry cooperative projects.

Kaj B. Jakobsen received the B.Sc.EE and the M.Sc.EE degree from the Technical University of Denmark, Kgs. Lyngby, in 1985 and 1986, respectively, the Ph.D. degree in Electrical Engineering from University of Dayton, Dayton, OH, in 1989, and the HD in Organization and Management, Copenhagen Business School, Copenhagen in 2000. From 1986-1989 he was a Fulbright Scholar at the Department of Electrical Engineering, University of Dayton, OH. Since 1990 he has been with the Department of Electrical Engineering, Technical University of Denmark, Kgs. Lyngby, where he is Associate Professor.

His research interests are in body-centric wireless network, wireless body area network, and body sensor network. He received in 1989 the NCR Stakeholder Award, Ohio, USA, and was appointed Teacher-of-the-Year at the Technical University of Denmark in 1994.